CHAPTER

FIVE

State selective electron capture by highly charged Xe ions

5.1 Introduction

Ever since the introduction of highly-charged ion sources, interactions between atoms and slow multicharged ions have been studied extensively. At low collision energies (keV), electron capture dominates the interaction dynamics and therefore it plays a significant role in fusion [9, 89] and astrophysical plasmas [2, 5] (solar wind). One-electron capture proceeds mainly by transfer of the most loosely bound atomic electron. Consequently one-electron models (see e.g. [49]) are used to describe electron capture processes at low energies, i.e. velocities well below the classical orbiting velocity of the active electron. Next to the real one-electron systems of fully stripped ions interacting with atomic hydrogen, quasi-one-electron systems like collisions of fully stripped low-Z ions with alkali atoms are amongst the most studied systems. One would like to investigate one-electron capture for higher-charged (q>+10) ions too. Intense enough beams of fully stripped ions such as for example Ar^{18+} can not be produced by our ECR ion source. However, for example closed-shell ions such as Xe^{18+} and Xe^{24+} are a good approximation of fully stripped Ar^{18+} and Cr^{24+}.

Here we present a systematic study of state selective one-electron capture in Xe^{18+}+Na($3s$) collisions at energies ranging from 0.5 to 3.35 keV/amu. As the classical orbiting velocity of the Na($3s$) electron corresponds to 9 keV/amu, our energies are below the regime where the processes dominating the interaction change from capture to ionization.

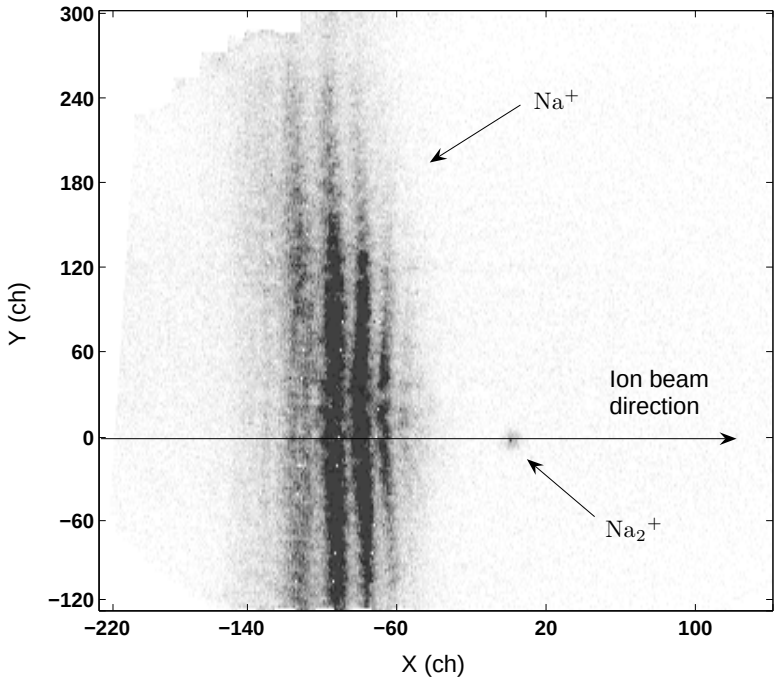

Figure 5.1: *XY-distribution of Na^+ recoils resulting from 1.67 keV/amu $^{129}Xe^{18+}$+Na collisions. The projectile direction is along the X-axis. The vertical bands are due to one-electron capture into different n-shells. Also the molecular sodium ions formed in the MOT are visible.*

5.2 Experimental results

The cooled cloud of sodium target atoms collected in our apparatus is crossed with a beam of Xe^{18+} or Xe^{24+} ions at different velocities. Compared with the measurements done with He^{2+} beams we increased the voltages on the extraction and focusing electrodes to the following values: $V_+ = +2.04$ V, $V_- = -4.92$ V, $V_1 = -3.4$ V, $V_2 = -2.7$ V, and $V_3 = -0.52$ V (cf. Fig. 3.13). The extracting electric field is increased in this way to 0.7 V/cm assuring that ions over the full range of recoil energies are collected on the detector. The higher fields are necessary because due to the high charge state of the Xe ions the recoil energies are relatively high. By increasing the extraction voltages the resolution decreases from 0.07 a.u. to 0.1 a.u., but this is still sufficient to distinguish the different capture channels.

From the 2D image on the detector (see Fig. 5.1) the recoil momentum vector can be reconstructed. Even for the higher extraction voltages used we do not collect

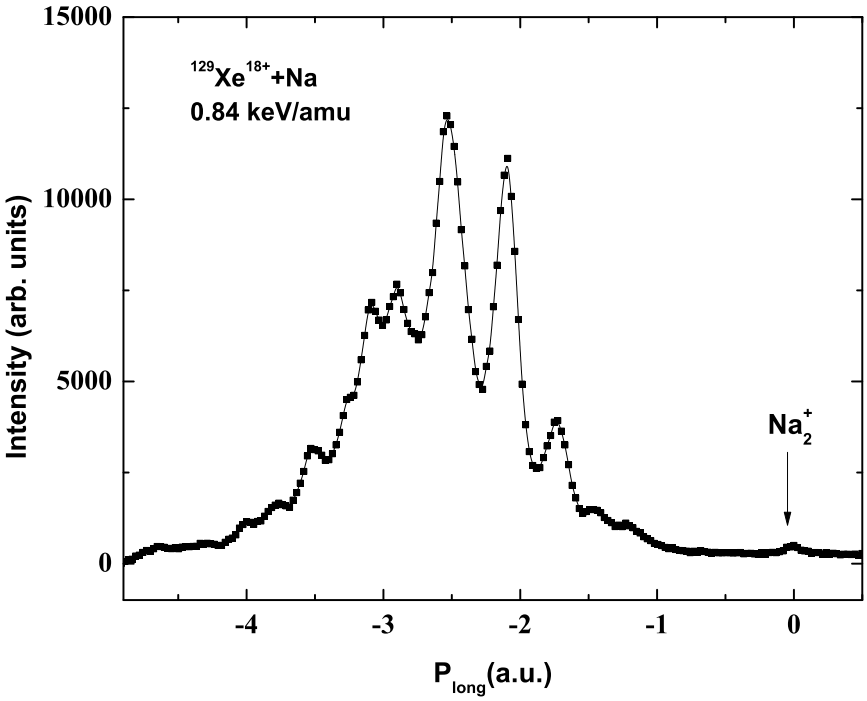

Figure 5.2: *The longitudinal momentum spectrum of 0.84 keV/amu $^{129}Xe^{18+}$+Na(3s) collisions.*

all the recoils on the detector. But due to the cylindrical symmetry of the system collecting only one half of the recoils is sufficient to obtain the Q-value spectrum.

For the higher longitudinal recoil momenta (p_{long} larger than -3 a.u.) we observe a splitting in the lines (see Fig. 5.1 and Fig. 5.2). The Wiley-McLaren focussing criterium is no longer valid. Recoils with high longitudinal momenta ejected either towards or away from the detector do not arrive on the same position on the detector. This splitting in the peak shapes can be reproduced by simulating the ion trajectories in our setup using the SIMION 8.0 code [77]. Fig. 5.3 shows the simulation for capture into Xe^{17+}(n=15) i.e., $p_{long} \sim 3a.u.$. The splitting between upward and downward recoiled ions is most obvious at Y=0 mm.

In order to obtain the longitudinal momentum recoil spectra in atomic units instead of channels we need to calibrate the spectra. To do this conversion from channels to atomic units we need at least 2 reference points for which we know the longitudinal momentum. One reference point is the position of the Na_2^+ ions which are due to the sodium molecular ions formed in the MOT cloud by associative ioniza-

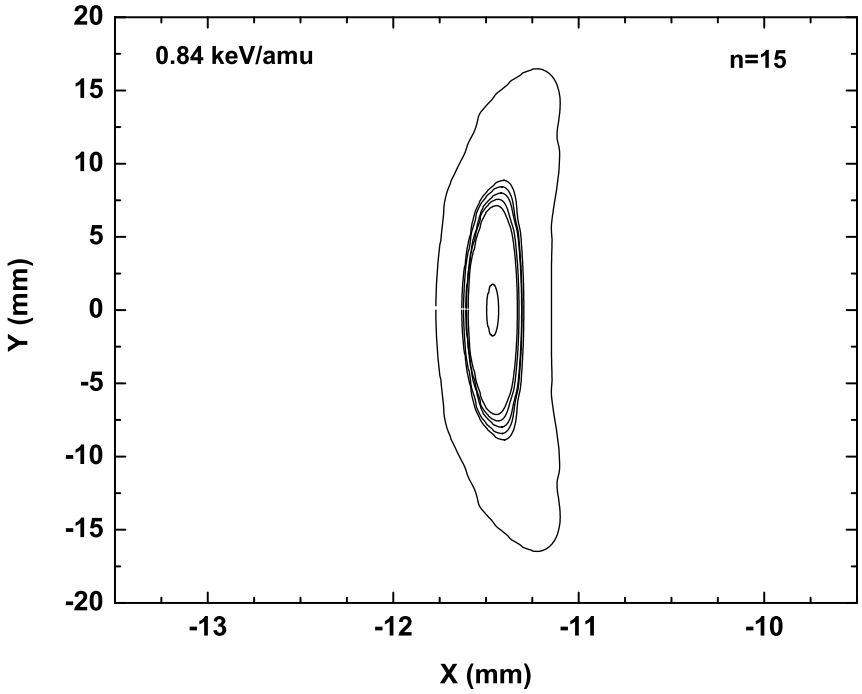

Figure 5.3: *A SIMION simulation of the recoil-ion position on the detector for capture into n=15 shell of $^{129}Xe^{17+}$ after 1.67 keV/amu $^{129}Xe^{18+}$+Na collisions.*

tion [84, 85]. They have negligible recoil momentum, which makes it safe to assume that the position of the molecular ions marks the position of the MOT cloud, and thus the zero point in the longitudinal momentum spectra. The second reference point needed is impossible to find in the Xe spectra because we do not know the exact shells into which capture occurs. Therefore, before each Xe measurement we do a measurement with O^{6+} for which the spectrum is well known [108]. From the measurement using O^{6+} we can obtain the conversion from channels to atomic units which we can apply to the subsequent Xe measurement. This procedure is quite easy to use, because we already have oxygen in the ion source where it is used as a mixing gas to increase the Xe^{18+} output. We just need to select the O^{6+} beam from the source, do the measurement (in a few minutes) and then switch back to the Xe ions.

From the longitudinal component of the Na^{+} recoil momentum, the Q-value of the collision can be obtained using equation 4.1.

The momentum resolution of 0.1 a.u. corresponds to a resolution of 1.2-2.2 eV

ion	n	$Q-value(eV)$		$p_{long}(a.u.)$	
		min	max	min	max
Xe^{18+}	13	-26.0	-20.9	-3.3	-2.7
	14	-21.3	-17.3	-2.8	-2.3
	15	-17.7	-14.4	-2.3	-1.9
	16	-14.7	-12.1	-2.0	-1.6
	17	-12.3	-10.1	-1.7	-1.4
	18	-10.3	-8.5	-1.4	-1.2
	19	-8.6	-7.1	-1.2	-1.0
	20	-7.2	-5.9	-1.0	-0.9
	21	-6.0	-4.9	-0.9	-0.7
Xe^{24+}	18	-21.2	-19.0	-2.77	-2.51
	19	-18.4	-16.6	-2.43	-2.20
	20	-16.0	-14.4	-2.13	-1.94
	21	-14.0	-12.6	-1.88	-1.71
	22	-12.2	-11.0	-1.66	-1.52
	23	-10.7	-9.7	-1.47	-1.35
	24	-9.3	-8.5	-1.31	-1.20

Table 5.1: *Q-values and longitudinal momenta for the relevant n shells in Xe^{18+}+Na(3s) → Xe^{17+}(n)+Na^{+} and Xe^{24+}+Na(3s) → Xe^{23+}(n)+Na^{+} for 2.23 keV/amu projectile energy. The "min" and "max" values correspond to l=0 and l=n-1, respectively.*

for the Q-value, depending on the projectile velocity. In Table 5.1 the Q-value limits of the relevant shells and the corresponding longitudinal momenta for collisions of Xe^{18+} and Xe^{24+} with ground state Na(3s) at 2.23 keV/amu are given.

A typical Q-value spectrum for Xe^{18+}+Na(3s) collisions is shown in Fig. 5.5. The main capture peak occurs at -12.15 eV. Such a Q value of -12.15 eV can correspond to Q_{min}(n=17) and Q_{max}(n=16), see table 5.1.

In the following it is indicated why we have chosen to identify the peak with Q_{max}(n=16). By means of the multi-configuration Hartree-Fock (MCHF) code [109] the binding energies of Xe^{17+}(nl) states up to n=9 could be calculated. The quantum defects associated with the different l states are 1.10, 0.96, 0.67, 0.32, 0.08, and 0.02 for l=0, 1, 2, 3, 4, and 5. For l>5 the quantum defects are basically 0, i.e., the l states take up hydrogenic binding energies. This implies that, for example, for Xe^{17+}(n=16) all l states with l$\geq$6 are degenerate. Fig. 5.4 shows a simulated spectrum for capture

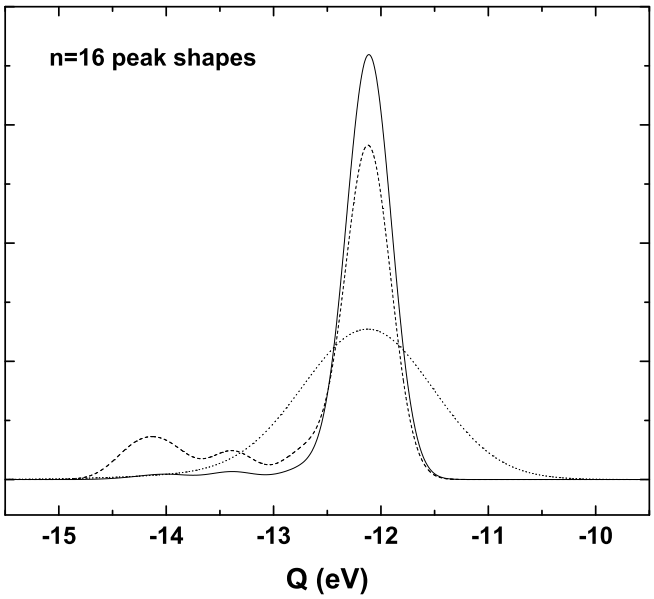

Figure 5.4: *Simulated spectrum for capture into Xe^{17+}(n=16) assuming an equal population of all l states and an experimental resolution of 0.5 eV (– –) and alternatively assuming a statistical population of the l states and an experimental resolution of 0.5 eV (—) and 1.5 eV (· · ·).*

into Xe^{17+}(n=16) assuming an equal population of all l states and an assumed experimental resolution of 0.5 eV (real experimental resolution is 1.2 eV). It is obvious that the spectrum peaks at a Q value very near to Q_{max}(n=16).

In the energy range of our experiments typical l distributions are not equal but rather statistical [1, 30, 110] which shifts the spectral weight even further to Q_{max}(n=16), see Fig. 5.4. The figure also shows the spectral shape for a statistical population and the experimental resolution of 1.5 eV. Given this near Gaussian shape we decided to fit the experimental spectra with Gaussian line shapes centered near Q_{max}.

In Fig. 5.5 the Q-value spectrum of Na^+ recoil ions resulting from 2.23 keV/amu Xe^{18+}+Na collisions is shown. From the Q-value spectra the relative cross sections for capture into the $n = 13$, $n = 14$, $n = 15$, $n = 16$, $n = 17$, $n = 18$ and $n = 19$ shells are obtained.

In the fitting procedure, for the lower n-shells two Gaussian curves are used to fit the lines due to the afore mentioned splitting in the lines. After fitting the dominant

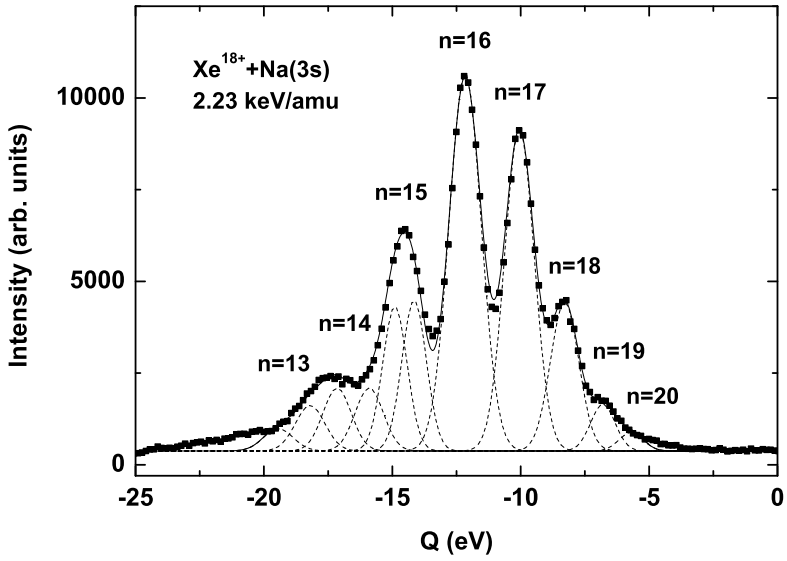

Figure 5.5: *Q-value spectrum of Na^+ recoil ions resulting from 2.23 keV/amu Xe^{18+}+Na collisions.*

channel $n = 16$ and finding the width of the line, the line widths of the higher n shells are slightly increased relative to the one of the $n = 16$ shell taking into account equation 4.2

The area of the lines S_n relative to the total number of counts S_{total} is a direct measure for the relative cross section:

$$\sigma_n^{\mathrm{rel}} = \frac{S_n}{S_{total}}. \tag{5.1}$$

The relative cross sections for one-electron capture from Na(3s) into $Xe^{17+}(n)$ for $n = 13 - 19$ are shown in Fig. 5.6(a).

With increasing collision energies, i.e. closer to the classical orbiting velocity of the Na(3s) electron, capture into higher n states becomes more favorable as seen in Fig. 5.6(b).

The higher charge state of the Xe^{24+} projectile ion is influencing the electron capture processes. One expects that capture processes will populate higher states in the projectile. This is evident from Fig. 5.7.

The relative cross sections for capture into the different n-shells are shown in Fig. 5.8(a). Capture into the $n = 21$ shell is the dominant channel over the full

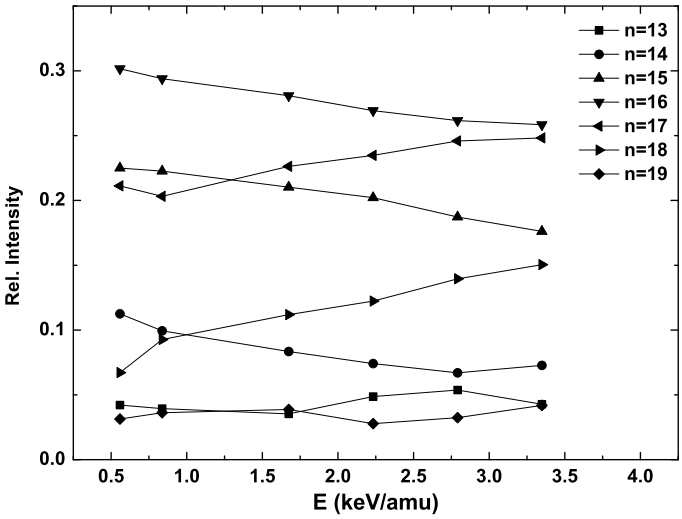

(a)

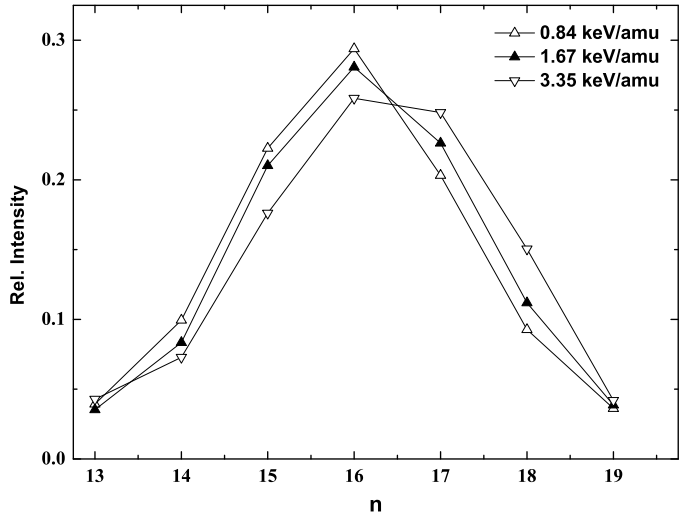

(b)

Figure 5.6: *(a) Relative cross sections for one-electron capture from Na(3s) into* $Xe^{17+}(n)$ *for* $n = 13 - 19$. *(b) n-state distribution for* Xe^{18+}*+Na(3s) collisions.*

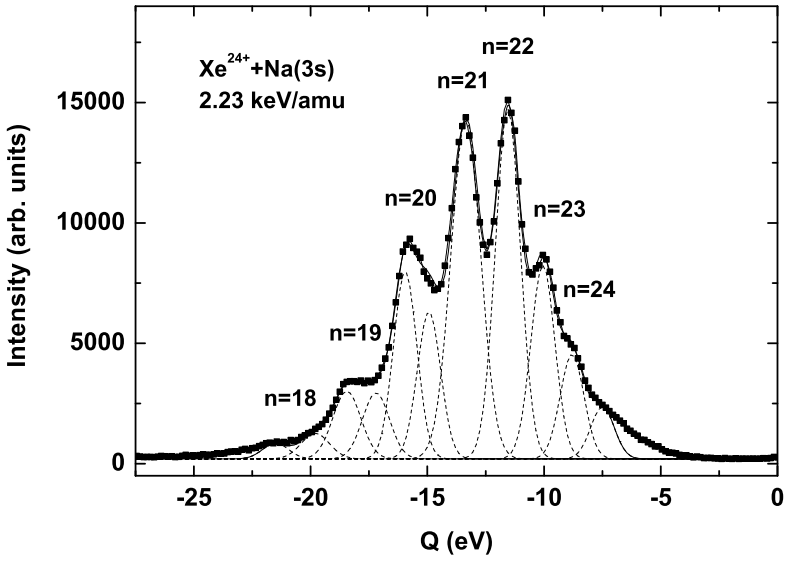

Figure 5.7: *Q-value spectrum of Na^+ recoil ions resulting from 2.23 keV/amu Xe^{24+}+Na(3s) collisions.*

range of investigated collision energies. As for Xe^{18+} the contribution of capture into higher n-shells becomes more significant at higher collision energies as seen in Fig. 5.8(b).

The CBM predicts the reaction window to be centered around

$$E_b = -I\left(1 + \frac{q-1}{1+2\sqrt{q}}\right) \tag{5.2}$$

where I is the ionization potential of Na(3s) and q is the charge state of the projectile ion. This corresponds for Xe^{18+} and Xe^{24+} to a binding energy of 14.4 eV and 16.1 eV respectively.

Taking a hydrogenic approximation for E_b, this binding energies correspond to a "classical" principal quantum number, n^*,

$$n^* = \frac{q}{\sqrt{2E_b}}, \tag{5.3}$$

Using equation 5.2 and 5.3 the main capture channels predicted by the CBM are n=17 for Xe^{18+} and respectively n=22 for Xe^{24+}. From the experimental results we see that capture occurs into the shell directly below the one estimated by

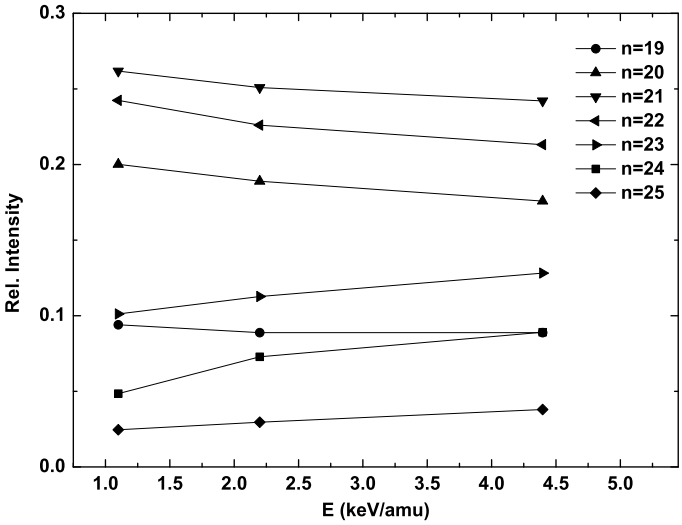

(a)

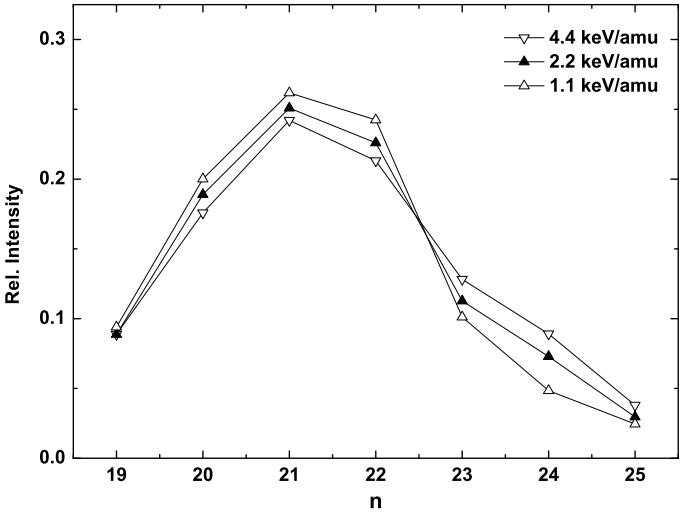

(b)

Figure 5.8: *(a) Relative cross sections for one-electron capture from Na(3s) into $Xe^{23+}(n)$ for $n = 19 - 25$. (b) n-state distribution for Xe^{24+}+Na(3s) collisions.*

CBM. Indications that for highly charged ions (q>10^+) the CBM may overestimate the n-value of the dominantly populated n shell are also found in Cl^{17+}+H [111] and Ar^{18+}+He [112].

5.2.1 Transverse momentum distributions

Transverse momentum distributions or differential cross sections (DCS) are extracted from the recoil spectra for capture into the $n = 14 - 19$ shells in the case of Xe^{18+} and $n = 20 - 23$ shells in the case of Xe^{24+}. Although DCS for H^++Na(3s,3p) [36], Li^++Na(3s,3p) [80] and O^{6+}+Na(3s) [113] have been studied intensively, for the highly charged ions and in particular for the present collision systems no experimental DCS have been reported before.

Relative differential cross sections as a function of scattering angle at 2.23 keV/amu for Xe^{18+} and Xe^{24+} are shown in Fig. 5.9 (a) respectively (b). All data are normalized to their peak maximum to facilitate the comparison between the different channels.

One observes that for both Xe^{18+} and Xe^{24+} capture into higher n-shells yields smaller transverse momentum, thus smaller scattering angle. This can be explained by the fact that capture into higher n-shells occurs at larger impact parameters thus the scattering angle is smaller.

When comparing the transverse momenta of the dominant n levels, one observes that the scattering angles in the case of Xe^{24+} are larger than for the Xe^{18+}. This is due to the fact that with higher charge state the repulsion is increased. When we consider the corresponding impact parameters (obtained using equation 2.23) it is observed that the dominant level is occupied at larger impact parameters for Xe^{24+} than for Xe^{18+}. That would yield smaller scattering angles. Apparently the stronger repulsion due to the higher charge prevails above the higher impact parameter.

5.3 Conclusions

Single-electron capture processes in Xe^{18+}+Na(3s) and Xe^{24+}+Na(3s) collisions at energies below the matching velocity have been studied experimentally. For Xe^{18+} impact on Na(3s) capture occurs predominantly into the $n = 16$ shell, i.e., the shell directly below the one estimated by CBM. At impact velocities closer to the classical orbiting velocity of the Na(3s) electron, capture into higher n states becomes more favorable for Xe^{18+}. In the case of Xe^{24+} capture into $n = 21$ is the main channel.

Transverse momentum distributions show that electron capture occurs at larger impact parameter but at the same time the scattering angles are larger for Xe^{24+} than for Xe^{18+} which can be explained by the higher charge state.

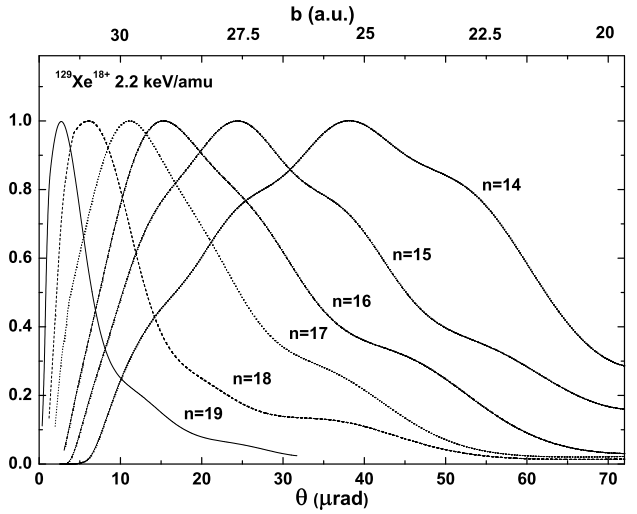

(a)

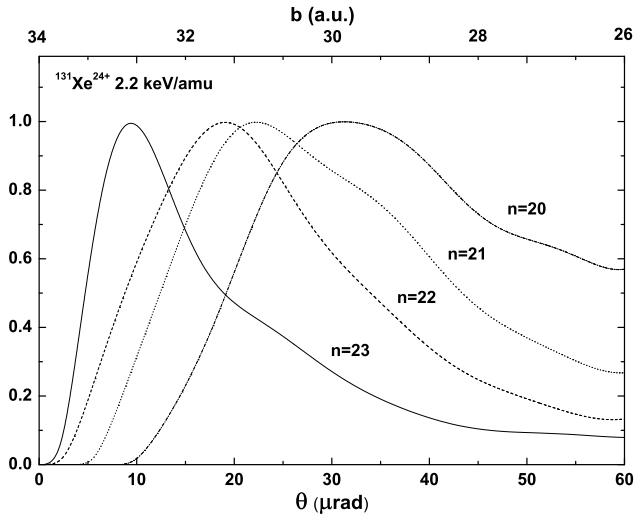

(b)

Figure 5.9: *Experimental transverse momentum distributions as a function of the scattering angle (lower scale) and impact parameter (upper scale) at 2.23 keV/amu for capture into $n = 14 - 19$ in Xe^{18+}+Na(3s) collisions (a) and for capture into $n = 20 - 23$ in Xe^{24+}+Na(3s) collisions (b). All distributions are normalized to their peak values.*